Title

Formation of Hydrogenated Amorphous Carbon Films of Controlled Hardness from a Methane Plasma

Journal

Physical review B, 41(5)

Authors

Vandentop, G.J.
Kawasaki, M.
Nix, R.M.
et al.

Publication Date

1989-10-01

LBL-27526
Preprint

Center for Advanced Materials

CAM

Submitted to Physical Review B

Formation of Hydrogenated Amorphous Carbon Films of Controlled Hardness from a Methane Plasma

G.J. Vandentop, M. Kawasaki, R.M. Nix, I.G. Brown,
M. Salmeron, and G.A. Somorjai

October 1989

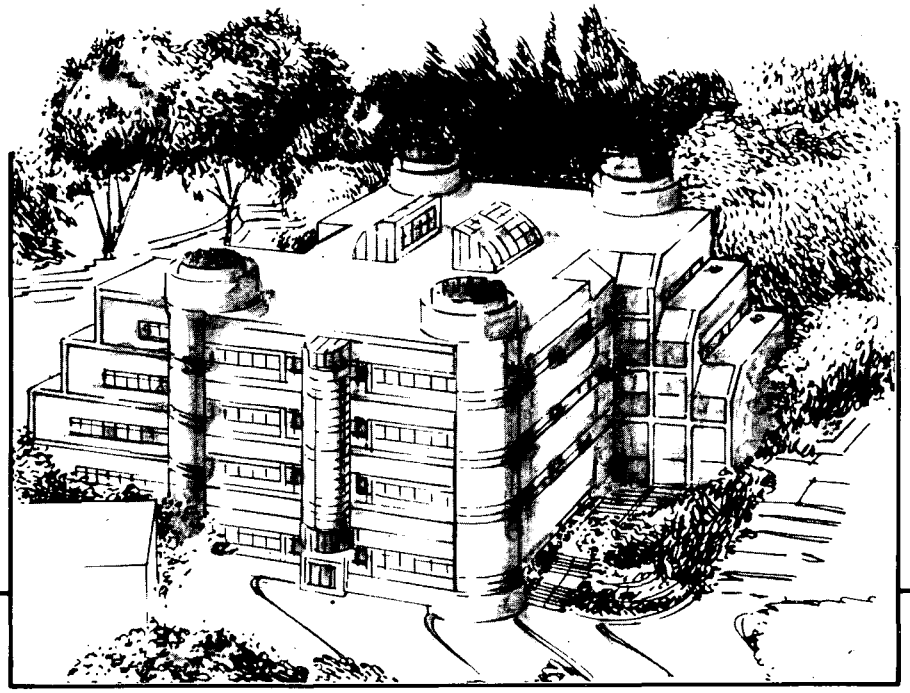

Materials and Chemical Sciences Division

Lawrence Berkeley Laboratory • University of California

ONE CYCLOTRON ROAD, BERKELEY, CA 94720 • (415) 486-4755

Prepared for the U.S. Department of Energy under Contract DE-AC03-76SF00098

DISCLAIMER

LBL-27526

Formation of Hydrogenated Amorphous Carbon Films of Controlled Hardness from a Methane Plasma

G.J. Vandentop M. Kawasaki R.M. Nix I.G. Brown
M. Salmeron G.A. Somorjai

October 18, 1989

Center for Advanced Materials
Materials and Chemical Sciences Division
Lawrence Berkeley Laboratory
1 Cyclotron Road
Berkeley, California 94720

and

Department of Chemistry
University of California
Berkeley, CA 94720

Abstract

Studies of amorphous hydrogenated carbon (a-C:H) film deposition revealed that methyl radicals are the precursor species responsible for the bulk mass deposition of the films, while the ions act to improve the mechanical properties. The films were deposited on Si(100) substrates both on the powered (negatively self-biased) and on the grounded electrodes from a methane rf plasma (13.56 MHz) at 68 to 70 mTorr and 300 to 370 K. The films produced on the powered electrode exhibited superior mechanical properties, such as high hardness. A mass spectrometer was used to identify neutral species and positive ions incident on the electrodes from the plasma, and also to measure ion energies. Methyl radicals were incident on the electrode surface with an estimated flux of $10^{16}cm^{-2}s^{-1}$, for an rf power of 50 W. Methyl radicals appear to be the dominant intermediates in the growth of the soft carbon polymer, and there is a remarkable decrease in deposition rate due to introduction of NO, a radical scavenger. A novel pulsed biasing technique was used so that the role of ions in the plasma could be studied separately. It was found that the hardness of the films depends on the power supplied by the ions to the growing film surface (the time averaged difference between the plasma potential and the electrode potential), but not on the energy of individual ions. The pulsed biasing technique offers an efficient method to adjust the film hardness by independent control of the neutral radical and ion fluxes to the surface.

1 INTRODUCTION

Amorphous hydrogenated carbon films (a-C:H) have been widely utilized in recent years as hard coatings with useful optical, thermal, and electrical properties. These films are usually deposited by plasma assisted chemical vapor deposition (PACVD), ion beam deposition, or sputter deposition. Identification and control of the parameters that determine the physical and chemical properties of these films is necessary if they are to be used in various applications. There are several relevant papers [1-18] that testify to the great number of investigations to characterize these films and determine what the necessary plasma conditions are that yield carbon films with the desired properties. However, correlation between the plasma deposition conditions and the film properties has been difficult to establish.

The purpose of our studies is to characterize both the plasma and the physical properties of the films to develop the scientific basis that will allow control over film properties. To that effect, properties of a-C:H films - hardness, scratch resistance, density, compressive stress, and FTIR spectra - were investigated and compared between the films produced on an rf powered electrode and on a grounded (nonpowered) electrode. These studies revealed the importance of high energy ion impact in creating desirable properties. Mass spectroscopic plasma characterization was performed to identify the neutral and ionic species in the plasma and to measure their concentrations. In order to deconvolute

the roles of the ions and radicals in the growth of the films, we have developed a novel high voltage pulsed biasing technique, and also investigated the effect of a radical scavenger, NO. Pulsed biasing offers a convenient way to change the energy and flux of ion bombardment without affecting the radical flux to the substrate, and allows a degree of control over the final properties of the films not attainable by conventional techniques. The role of radicals in film growth was also studied by reducing the radical flux by the addition of NO. As a result of these studies it was uncovered that neutral methyl groups are the precursors for forming a soft polymer film and that ion bombardment causes hardening. Polymer film deposition rate and ion hardening can be controlled independently by means of pulsed biasing.

2 EXPERIMENTAL PROCEDURES

2.1 The Plasma Deposition System and Mass Spectrometric Analysis

The carbon films in this study were produced by PACVD using methane gas in an rf apparatus (frequency 13.56 MHz) with a parallel plate configuration as schematically illustrated in Fig.1. The plates were 8.75 cm in diameter with a separation distance of 2.0 cm. The plates were housed in a stainless steel chamber pumped by a Seargent Welch model 1397 mechanical pump to a base pressure less than 10 mTorr, as measured with a Baratron type 227AHS-C-10 capacitance manometer. Methane gas (Matheson 99.5%) was used as the feedstock and gases were introduced into the plasma region through an orifice in

the upper electrode. Methane flow rates were measured with Porter Mass flow controllers as approximately 8 cm^3/min. The initial methane pressure before plasma discharge was adjusted to 65 mTorr. Upon initiation of discharge the gas pressure rose to 68-70 mTorr, depending on rf power. Typically rf power was applied to the lower electrode while the upper electrode was grounded, but the connection was reversed when mass spectrometric analysis of the species impinging on the grounded electrode was desired. Single crystal Si(100) wafers, 0.338 mm thick, were used as substrates. The wafers were etched in 49% HF immediately before being attached to the electrodes.

The plasma chamber was connected through a differentially pumped middle stage to a high vacuum chamber in which was installed a UTI model 100C mass analyzer along with ion deflection lenses to measure the ion energy distributions. The first orifice through the lower electrode in the plasma chamber was approximately 100 μm in diameter, while the second orifice, between the middle stage and the lower high vacuum chamber, was about 1 mm in diameter. Pressure was maintained on the order of 10^{-8} Torr in the lower chamber. The ion deflection lenses were made of two metal plates, separated by 5 mm, with the center holes 3 mm in diameter. To minimize undesirable off-axis deflection of ions, the upper plate was grounded and the retardation voltage was applied to the lower plate so that the ion retarding field was confined between the plates. For the same reason, these lenses were placed as close as possible to the mass analyzer.

A high voltage pulse generator system used for the pulse biasing of the grounded electrode was constructed in this laboratory, and is capable of producing negative pulses of more than 1 kV with a pulse width of about 2 μs, at frequencies less than 30 kHz. The frequency limit was increased up to 100 kHz for negative voltages less than 80 V, by making use of only the trigger pulse generator in this system.

The mass spectra for the neutral species were taken under the normal ionizer-on operation, with electron energy of 75 eV and ion energy of 19 eV. Every component in the ionization chamber was grounded while taking ion spectra, except for an ion focusing lens (ionizer-off operation). When the total ion intensity was measured, the quadrapole filter elements were also grounded.

A quantity of key interest in this study is the potential drop between the plasma glow region and the sample surface. For a sample on the powered electrode, the potential drop is the difference between the plasma potential and the self-bias potential at that electrode. The rf powered electrode acquires a negative self-bias voltage with respect to the plasma potential, due to the large difference in ion versus electron mobilities[19]. For our parallel plate electrode system, the self-bias voltage varies with applied rf power as shown in Fig. 2.

With the plasma ignited, a steady state potential distribution is established between the electrodes. Fig.3 shows how the plasma potential is expected to vary across the inter-electrode gap for an rf power of 50 W. The sheath width in this figure is based on a Debye shielding length (about 2 mm), as estimated from

an exponential curve fitting of the floating potential profile as measured with a Langmuir type probe[20]. There is of course a significant difference between the floating potential and the plasma potential, but Fig.3 correlates well with the width of the cathode dark space (a little less than 1 cm) which could be observed visually through a window in the plasma chamber. The plasma potential in the glow space in Fig.3 is based on the average energy of ions incident on the grounded electrode, presented later in Fig.14.

It is evident from Fig.3 that positive ions created in the plasma region are accelerated towards both electrodes. However, the situation is very asymmetric, as positive ions striking the powered electrode can have as much as 400 eV of energy, while those striking the grounded electrode will have an energy close to 15 eV.

2.2 Film Characterization

The thickness of deposited films was measured by a Clevite Surfanalyser 150 profilometer, with a diamond tip being scanned across the step between the film and an area which had been masked during deposition. The profilometer was also used to measure the degree of bending of the silicon substrate, induced by the stress in the deposited films. From the bending radius, the thickness and Young's modulus of the substrate, the compressive stress within the deposited film was calculated by a conventional formula[21]. The density of the films was determined from the measured mass of the film and its volume. The Knoop

hardness of the films was measured with a Buehler Micromet microhardness tester with loads from 20 to 5 grams for films thicker than 1 μm. The ratio of the longer indentation diagonal to indentation depth for a Knoop indenter is 1:28. Indentation diagonal lengths of less than 10 μm were measured by Secondary Electron Microscopy (SEM). The scratch adhesion tests were performed on an apparatus described previously[22] and scratch tracks were observed by SEM and Auger Electron Spectroscopy (AES). FTIR spectra were obtained on a FTIR spectrometer operated under its transmission mode.

3 RESULTS

3.1 Film Growth Rate

Deposition rate in terms of thickness per unit deposition time is given in Fig.4 as a function of rf power. For our standard deposition conditions, with an rf power of 50 W, deposition rates were measured as 140 Å/min on the powered electrode and 95 Å/min on the grounded electrode. As will be shown in the next section, the density of the films produced on the powered electrode is greater than the density of films formed on the grounded electrode by about 30 %, which makes the mass deposition rate on the powered electrode twice as large as that on the grounded electrode. As can be seen in Fig.4, the deposition rate is not a linear function of rf power and tends to level off after 50 W. It should be noted that the measured deposition rate did not depend on whether the upper or lower electrode was powered. The difference in deposition rates

between the powered and grounded electrodes, as shown in Fig.4, is therefore not due to a gas flow effect, even though the methane is flowing into the plasma out of the upper electrode, making the system somewhat asymmetric.

3.2 Mechanical Properties, Film Thickness, and Density

The Knoop hardness value for the films formed on the powered electrode (PE, 34 GPa = 3468 kg/mm^2) are about fifteen times that for films formed on the grounded electrode (GE, 2 GPa = 0.24 kg/mm^2), and nearly one third that of diamond, as shown in Table 1. SEM images showed that films formed on the grounded electrode were much more susceptible to damage by scratch adhesion testing than were films formed on the powered electrode. Powered electrode films were not noticeably damaged by an 831g SAT test, as observed by SEM (Fig.5.). Films formed on the grounded electrode were severely damaged with a load of 831g, and damage was noticeable by SEM at load values as low as 32g. Relatively large areas (1mm diameter), centered on the scratch tracks, were depth profiled and AES was performed both in the track and away from the track. Fig.6 shows the Si and C AES signal intensities as a function of depth, demonstrating the elemental composition in and away from the scratch. The film formed on the powered electrode was not noticeably damaged at this load level, demonstrating its hardness and strong adhesion. The film formed on the grounded electrode, however, shows a large amount of damage and a strong intermixing of carbon and silicon in the scratch track, demonstrating the poor

mechanical properties of this film.

A markedly high compressive stress was measured for films formed on the powered electrode (Table 1). In order for the films to withstand such a high stress and remain attached to the silicon substrate, there must be good adhesion, probably due to strong Si-C chemical bonds which are expected to be present at the interface.

Density is also significantly different between the films produced on the two types of electrodes. The value for the carbon film produced on the powered electrode; 1.7 g/cm^3, is in close agreement with those previously reported[23]. Although this value is much lower than that of diamond (given also in Table 1 for reference), this does not imply that the film has a sparse three dimensional structure. In view of the considerable hydrogen content expected in these films, the number density (number of atoms per unit volume) could be close to that of diamond, and hard a-C:H films must essentially consist of a dense hydrocarbon phase[24].

3.3 FTIR Spectra and Film Composition

Fourier transform infrared spectroscopy of a-C:H films was carried out in order to study the hydrogen content and bonding within the films. Fig.7 compares the FTIR spectra of carbon films formed on the powered and on the grounded electrodes, in two frequency regions associated with C-H stretching and C-H bending vibrations. The soft carbon film shows absorption bands characteristic

of methyl groups (1375, 2878, and 2958 cm^{-1}) as well as methylene groups (1460, 2930 cm^{-1})[25]. The frequency of the above bands are close to those reported for alkanes[25], implying that the carbon films formed on the grounded electrode are made up of a structure which is predominantly polymer-like. It is also likely that they are composed of grains with methyl group rich boundaries, due to the large intensity of the methyl group bands.

In comparison, the carbon films formed on the powered electrode show no such distinct CH_3 bands, indicating that the amorphous hydrocarbon network extends over a significant range. The broad C-H stretching band at around 2920 cm^{-1} is similar to that reported by Dischler et al[26] for an a-C:H film produced from benzene by PACVD. In that study, the band was deconvoluted into four overlapping bands associated with sp^2 CH and sp^3 CH_2 stretching vibrations. On the bending region, a red shift of the CH_2 band is observed, 1445 cm^{-1} vs. 1460 cm^{-1} for the grounded electrode carbon film which, is suggestive of cyclization of the carbon skeleton[25]. Cyclization will promote extension of the three dimensional network and will cause stress inside the films. Moreover, the appearance of a weak band near 1600 cm^{-1} could be associated with graphite-like or conjugated sp^2 clusters, which must also be responsible for the strong absorption of visible light by the carbon films produced on the powered electrode.

The FTIR spectra also suggest a large difference in hydrogen content between the two films. Based on the molar extinction coefficients for the methy-

lene and methyl bending vibrations (14.9 and 15.0 l/mole-cm according to the work of Tibbitt et al[27]), the concentration of methyl and methylene groups in the carbon produced on the grounded electrode are estimated to be 12 and 20 mmole per gram of film (mmole/g_f), respectively. For the carbon film formed on the powered electrode, on the other hand, the methylene concentration is estimated to be about 5 mmole/g_f, lower by a factor of four than that in the grounded electrode carbon, while the methyl concentration is below the limit of detection. The lack of information for tertiary C-H groups does not allow evaluation of total hydrogen content, but, from the values given, a much lower hydrogen content is evident for the carbon film formed on the powered electrode.

3.4 Mass Spectrometric Plasma Studies

3.4.1 Neutral Radicals in Methane Plasma

In order to understand the contribution of radical species in a-C:H film growth, mass spectra of the neutral species incident on the powered and grounded electrodes were collected, as shown in Fig.8. The signal in the 12 to 15 amu range contains minor contributions from plasma radicals, as will be deduced later. The methane peaks have decreased to about half that observed before ignition of the plasma discharge and, instead, a strong molecular hydrogen peak and weak features due to C_2H_x species have emerged as a result of plasma reactions. Cracking patterns and sensitivities of the mass analyzer for all the relevant hydrocarbon species were measured in this system in advance, by leaking through

the pure gases from measured pressures in the plasma chamber. According to these calibrations, the weak features from C_2 species can be deconvoluted into the contributions from ethane, ethylene, and acetylene as shown in Fig.9, which is calculated for the spectrum obtained through the grounded electrode. A deconvolution of the features for the powered electrode resulted in a similar ratio. The main production channels of these stable C_2 species in a methane plasma have been discussed by Tachibana et al[16].

The sum of the partial pressures of the measured plasma species must coincide with the measured pressure in the system. Once the intensities resulting from the specific species are known, their respective partial pressures can be obtained by means of the cracking patterns and analyser sensitivities as measured for the pure compounds. The result is shown in Fig.10. This figure represents the partial pressures within a mean free path of the sampling orifice in the lower electrode. As can be seen in Fig.10, there is a measurable difference between the powered and grounded electrodes in terms of the individual partial pressures. However, summation of the partial pressures evaluated in this way results in an almost identical total pressure for both electrodes (ca. 65 mTorr), which is only about 3 mTorr below that measured with a capacitance manometer at a point away from the plasma region. This indicates a homogeneous total gas pressure within the plasma chamber, and provides an independent assessment of the mass analyzer system calibration.

Of great interest is the contribution made by the radicals, to the neutral

signal intensity. This contribution, neglected in Fig. 10, can partly account for the slightly higher total pressure measured with the pressure gauge, as compared to the calculated one. The mass signals due to radical species in the 12 to 15 amu range can be deduced by careful subtraction of non-radical components, namely the signal intensities due to the fragments of methane and C_2 species, produced in the mass spectrometer ionization chamber. The result is shown in Fig.11. The only signal observed at a level significantly greater than the experimental variation is that of 15 amu, showing that the methyl radical is dominant. This is in agreement with the predictions of Tachibana et al[16] and Kline et al[28]. Fig.11 also indicates that there is no significant difference in radical flux between the powered and grounded electrodes. From these data we can conclude that the flux of radicals produced in the plasma is not significantly different between the powered and grounded electrodes.

In order for the result shown in Fig.11 to be used for an estimation of the methyl radical density in our methane plasma, some information about the sticking coefficient of methyl radicals is required. The signal intensity measured with the mass analyzer depends on a steady state concentration of the relevant species in the high vacuum chamber for the mass analysis. This concentration is not solely determined by the flux of the species coming in through the orifice, but depends as well on the sticking probability onto the chamber walls.The pressure inside the chamber is maintained at 10^{-8} Torr, making collisions with walls the predominant scattering mechanism.

By blocking the direct pathway between the lower orifice and the mass spectrometer ionization chamber, the signal intensity of any species with a high sticking probability would be significantly attenuated. Fig.12 compares the relative radical intensities with and without such a shield. Only a slight decrease in the CH_3 signal intensity is observed when such a shield is in place. The difference is almost within the experimental variation. This indicates a fairly small sticking coefficient for the methyl radicals onto the stainless steel chamber walls, which in turn allows an estimation of methyl radical density in the plasma. The ionization cross section of the methyl radical is the only other important parameter to be taken into account. This will be explained in more detail in the discussion section, in relation to the deposition rate.

3.4.2 Ionized Species in Methane Plasma

The mass spectra of positive ions incident on the powered and grounded electrodes could be measured by turning off the ionizer in the mass spectrometer. The spectra are shown in Fig.13. In addition to the the primary ions CH_3^+ and CH_4^+ which are species produced by electron impact ionization of methane, secondary ions are also observed in relatively high ratios at the grounded electrode. These secondary ions, like CH_5^+ and $C_2H_5^+$, are produced through ion molecule reactions. On the other hand, at the powered electrode, CH_3^+ is the most dominant and even less hydrogenated CH_2^+ and CH^+ ions can be seen, together with minor peaks due to secondary ions as mentioned above.

The large difference in spectral features, as seen in Fig.13, can be explained

in terms of the larger potential drop near the powered electrode, as compared to the grounded electrode. Because of the large negative potential drop at the powered electrode, secondary electrons emitted there are accelerated into the plasma at much greater energies than those emitted at the grounded electrode. As a result, electron impact ionization of methane occurs at a much higher electron energy near the powered electrode. This is more likely to produce less-hydrogenated fragment ions. Also, ions produced through electron impact near the powered electrode are much more rapidly accelerated towards the electrode by the large potential drop than are ions produced near the grounded electrode. The probability that ions formed near the powered electrode react with methane molecules is thus decreased and the relative flux of the secondary ions onto the powered electrode is reduced.

Another difference between the two electrodes is the total ion intensity which is about a factor of ten less at the grounded electrode than at the powered electrode. This could in part be due to a higher ion flux at the powered electrode. However, care should be taken because the signal intensity measured with the mass analyser could also be influenced by other factors. In particular, the ions detected are those passing within a small solid angle which is roughly defined by the angle that the second orifice makes with the center of the first orifice at the lower electrode. Consequently, the angular distribution and the degree of focussing of the ions after passing through the first orifice could significantly affect the signal intensity. More direct measurements of total ion flux are cur-

rently underway.

By measuring and differentiating the ion signal intensity as a function of retarding voltage, we could obtain the ion energy distributions with respect to the ground potential of the mass spectrometer. Fig.14 shows the ion energy distributions measured in this way for CH_3^+, H_2^+, as well as for the total ions. In the case of the grounded electrode, the energy peaks are found, irrespective of the species, in the 15 to 20 eV range. This corresponds to the plasma potential in the glow space as shown in Fig 3.

Since the mass spectrometer and all other chamber elements located below the orifice in the lower electrode are at ground potential, ions incident on the lower electrode with energies from 350 to 430 eV decelerate to energies from 0 to 80 eV before being detected. Therefore, the energies with which ions strike the powered electrode are 350 eV higher than the energies shown in Fig. 14. The ion energy distributions for the powered electrode are also more complex than that for the grounded electrode. The distribution for light hydrogen ions, for example, shows a high energy peak together with a secondary peak on the low energy side. This is likely to be related to an rf modulation of ion energy, which takes place when the time required for an ion to traverse the cathode sheath is comparable to or shorter than the rf cycle. In fact, a much heavier ion, $CH_3{}^+$, shows only a single energy peak close to the plasma potential. This last point implies that ions which have entered the sheath edge impinge on the powered electrode with a kinetic energy almost equivalent to the potential

difference between the electrode and the plasma bulk, without any significant loss of energy due to collision with gas phase species. Thus, the kinetic energy of ions impinging on the grounded electrode should be less than 20 eV on average, but exceeds 350 eV for ions incident on the powered electrode.

3.5 Alteration of a-C:H Film Properties by Plasma Control

3.5.1 Pulsed biasing of the Grounded Electrode

The data up to this point suggests that the significant difference in the growth conditions between the powered and grounded electrodes is the relatively high flux and energy of the ions impinging on the rf powered electrode. Since the films formed at the powered electrode are mechanically superior to those formed at the grounded electrode, ion impact processes must be at the origin of the hardness of these films.

We have devised a pulsed biasing experiment to enhance and control ion bombardment onto the otherwise grounded (nonpowered) electrode in order to illuminate the effect of the ions more clearly. By pulsing the nonpowered electrode to large negative voltages during the deposition, we can control the flux and energy of the incident ions and create conditions at the nonpowered electrode more similar to those at the powered electrode. This control, unlike the rf power control conventionally used to vary ion energy, has a relatively small effect on the radical flux, as long as the pulse width and frequency are varied so that the nonpowered electrode is near ground potential most of the

time. A similar technique, but with pulse heights from 10 - 100 keV, has been employed by Conrad and Castagna[29] for ion implantation. Our technique employs pulses of much lower voltage, thus bombarding the surface with ions of much lower energies and not implanting the ions in the traditional sense.

As a convenient parameter for the pulsed biasing under these conditions, we chose the time averaged potential drop at the pulsed electrode, namely the time averaged potential difference between the plasma bulk and the electrode. If we assume the ion flux to be roughly constant, this parameter is proportional to the total power supplied by ions onto the growing film surface. Fig.15(a) shows how the thickness deposition rate of the film varies with the pulsing parameter defined above. The thickness deposition rate decreases with the average potential drop, but the mass deposition rate remains constant. Therefore, it appears that the ions act to densify the films. The decrease in the thickness deposition rate by the pulse biasing is in remarkable contrast to the situation on the powered electrode, where the deposition rate was significantly greater than that on the grounded electrode (cf. Fig.2)

The Knoop hardness of the films increases monotonically with the average potential drop (Fig. 15(b)). The compressive stress becomes apparent after the average potential drop exceeds 50 V. Data points on this plot are listed for widely varying pulse peak voltages, and no dependance on peak voltage is apparent. Thus, we reach one of the most important conclusions of this study; that the increase of hardness depends predominantly on the power supplied by

the ions to the growing film, but not on the energy of individual ion. Also significant is the fact that, in spite of the considerable hardness increase, up to one half that achieved on the powered electrode, no increase in the deposition rate was observed, implying a relatively large contribution of radicals to the bulk mass deposition of the films.

3.5.2 Inhibition of Carbon Film Growth by NO Scavenging of Radicals

The studies utilizing the pulsed biasing technique show the hardening effect of ion energy and also indicate a relatively large contribution of radicals to the bulk mass of the films. In order to further clarify the radical contribution to film growth, the effect of a radical scavenger on growth rates was studied. It has been demonstrated in the case of silicon growth by PACVD, that the addition of a small amount of radical scavenger into the plasma causes a large decrease in the deposition rate[30]. Fig. 16 shows the effect of NO, a radical scavenger, on the deposition rate of a-C:H films. Here the total gas pressure before plasma ignition was kept constant at 65 mTorr as before, in order to avoid large changes of plasma parameters. Although this caused a decrease in methane pressure, it amounted to only 20% for the maximum NO content. Therefore this effect can account for only a moderate decrease in the deposition rate. In Fig.17, a very strong decrease in growth rate is evident in the case of the powered electrode, where as little as 5% NO decreases the growth rate by more than a factor of two, and no deposition was observed in the presence of

20% NO. A decrease in growth rate is also measured for the film grown on the grounded electrode, however this decrease is less rapid.

Auger electron spectroscopy was performed on a film formed with the addition of 10% NO to the plasma. It was clear that a large amount of nitrogen and oxygen had been incorporated into the film formed on the grounded electrode. It is apparent that the product of radical scavenging, some sort of CNO polymer has been deposited at the grounded electrode. AES also demonstrated very little if any NO incorporation into the film formed at the powered electrode. The additional presence of the CNO polymer at the grounded electrode accounts for the less rapid decrease in deposition rate there, as compared to the rate at the powered electrode. The CNO polymer is susceptible to decomposition by ion bombardment, hence its absence at the powered electrode.

It is important to demonstrate that NO is not scavenging the ions as well as the radicals. Fig.17 shows the mass spectra of ions incident on the powered electrode with and without the addition of NO (20%). The intensity of the ion signal has decreased by about a factor of two with the addition of 20% NO. However, as is seen in Fig.16 the growth rate of the films has decreased to zero at this point. If the ions were the predominant precursor, we should still see a growth rate on the order of 80Å/min. Hence we can conclude that it is a radical scavenging effect, not an ion scavenging effect, that accounts for the decrease in growth rate by the addition of NO.

This study shows once again how radicals in the plasma must be the pre-

cursors responsible for the deposition of the majority of the film mass.

4 DISCUSSION

4.1 Role of Radicals

The most dominant radical is the methyl radical (Fig. 11), which possesses a rather small sticking coefficient, as noted by the lack of intensity decrease with a shield in place (Fig. 12). The dominance of methyl radicals is expected from the individual cross section data by Melton and Rudolph[31], which favors the formation of methyl radicals over other fragments by electron impact dissociation of methane. Methyl radical abundance is consistent with a low reactivity of methyl radicals with methane which results in a long lifetime [10]. If the main role of the radicals is to provide the bulk mass of the films by polymerization, the methyl radical density must be high enough to account for the observed mass deposition rate. In order to evaluate this methyl radical density based on the result shown in Fig.11, the ionization cross section of methyl radical in our mass analyzer must first be estimated. The only available cross section data for methyl radical related species are for the deuterated species, CD_3, reported by Baiocchi et al[32]. For an electron energy of 75 eV, like that used in our mass spectrometer system, the total ionization cross section of CD_3 is about 2.8×10^{-16} cm^2. We will assume a similar cross section for CH_3. On the other hand, the total ionization cross section of methane, which we used as a reference species for the present estimation, varies significantly as determined by differ-

ent workers. We chose the value of 3.8×10^{-16} cm^2, as reported by Melton et al [31]. Using the same intensity units as used in Fig.11 , 1 mTorr of methane in the plasma chamber produces an integrated intensity over the total ionization fragments of about 2.0, while according to Fig.11, the signal intensity due to methyl radical is approximately 0.2.

Due to the small sticking probability of the methyl radical with the chamber walls, its average residence time in the high vacuum chamber where mass analysis occurs, is expected to be similar to that of the stable methane molecule. Therefore the numerical values given above are sufficient for estimating the methyl radical density in the methane plasma. From the signal intensity ratios and the ionization cross sections used, the partial pressure of methyl radical should be about 0.14 mTorr, which is equal to a radical density of 4.5×10^{12} cm^{-3} at 300 K. For this density, the radical flux to the substrate is calculated to be about 7×10^{16} $cm^{-2}s^{-1}$.

The mass deposition rate, as measured on the powered electrode, for example, was 4.1×10^{-8} $gcm^{-2}s^{-1}$. By assuming an atomic ratio of hydrogen to carbon in the film to be 1:1, the above growth rate requires deposition of C_1 species at the rate of 1.9×10^{15} $cm^{-2}s^{-1}$. Due to the much lower atomic mass of hydrogen as compared to carbon, this value is not very sensitive to what atomic ratio of hydrogen is assumed. A similar calculation for the grounded electrode leads to a smaller rate of 1.0×10^{15} $cm^{-2}s^{-1}$.

A comparison of the estimated radical flux with these growth rates shows

that methyl radicals alone adequately account for the deposited mass. Thus we determine a consistent sticking probability of methyl radical with the film surface, namely 0.02 to 0.03, calculated as the ratio of the deposition rate, in terms of the number of carbon atoms, to the methyl radical flux.

The methyl radical density estimated here can be compared to that recently reported by Toyoda et al[33], i.e., 4.7×10^{11} cm^{-3} for an rf power of 25 W at 10 mTorr. In view of the lower pressure and rf power used by these authors, the value is in relatively good agreement with that estimated here. They predicted that the sticking probability of CH_3 radicals with the chamber walls would be less than 10^{-3}. This is also consistent with our results, as the sticking coefficient of methyl radicals with the energetic film surface may be higher than that for collisions with the chamber walls.

4.2 Role of Ions

Ions act to modify the structure of a-C:H films making it harder and stronger. Pulsed biasing experiments indicated that the mechanical properties are varied by the difference between the plasma potential and the time averaged electrode potential, not by the individual ion energies. Thus, only the power supplied by ions to the growing film surface is crucial. This suggests a mechanism involving large but local thermal spikes quenched rapidly by the bulk of the film as proposed by Weissmantel[34]. Within these energetic spike regions, various processes - bond rearrangement, cross linking accompanied by hydrogen elimi-

nation, partial graphitization , etc. - could be highly activated. Each of these processes can respectively contribute to nanometer scale surface smoothness, high hardness and densification, small optical gap, etc., which are all characteristic of diamondlike a-C:H films. Also, a rapid quenching of the energetic surface layer by the bulk of the film is likely to be related to the high residual compressive stress, as nonequilibrium structures could be frozen out of the energetic surface.

It should be noted that the contribution of ions to increase the bulk mass of the film has not been totally ruled out. Indeed, in the ion beam deposition process, they are the only source of the bulk mass of the film. The larger deposition rate on the powered electrode as compared to the grounded electrode may be in some part due to the contribution of ions. Alternatively, the higher deposition rate on the powered electrode may be interpreted in terms of a potentially higher sticking coefficient for methyl radicals on a surface which is under the high energy ion impact, as is the case at the powered electrode. The measurement of the absolute ion flux onto the growing film surface will help us answer this question.

5 CONCLUSIONS

a-C:H films formed on the rf powered electrode have mechanical properties much superior to those formed on the grounded electrode. FTIR spectra suggest that the films formed on the grounded electrode have a polymer-like structure,

possibly composed of grains with boundaries rich in methyl groups. The films formed on the powered electrode, in contrast, show no distinct CH_3 related bands and thus likely consists of a three dimensional network of cyclic carbon skeletons.

The pulsed biasing experiment allowed us to determine the role of ions and demonstrated that both ions and radicals are intimately involved in the growth mechanisms of a-C:H films. Ion bombardment of the growing surfaces of a-C:H films alters the structure in a way which increases the hardness and density of these films. The film hardening is a function mainly of the difference between the plasma potential and the time averaged electrode potential, not of the height of the individual pulse. Thus the important quantity is the power supplied to the film surface by ions during deposition, not on the energy of the individual ion. This dependence may suggest a thermal spike and rapid quenching mechanism, resulting in the formation of metastable structures necessary for the production of films with desirable properties.

Methyl radicals were detected with an estimated radical flux of the order of 10^{16} cm^{-3}, which accounts for the measured mass deposition rate. Film mass is a function mainly of the integrated radical flux incident on the substrate. Addition of a radical scavenger dramatically decreases the growth rate of a-C:H films. Thus, radical species are an important precursor for film growth, as they provide the most significant feedstock for the bulk mass of the films.

Knowledge of the separate roles of radicals and ions opens a way to control

the deposition rate and film properties independently. The pulsed biasing of the otherwise grounded electrode is a simple and efficient method for this control.

In the future , we shall explore the structure of the interface and the adhesion between the film and substrate. Interfacial studies are already underway in our laboratory using a variety of surface science techniques, and the results will be reported soon.

6 ACKNOWLEDGEMENTS

This work was supported by the Director, Office of Energy Research, Office of Basic Sciences, Materials Science Division of the U.S. Department of Energy under Contract No. DE-AC03-76F00098. Additional support of the work was provided by the ICI company. The authors would like to thank Greg Blackman and Bharat Bhushan for helpful discussion and Michael Rubin for use of the FTIR spectrometer.

7 REFERENCES

1. H. Tsai, and D.B. Bogy, J. Vac. Sci. Technol. A 5(6), 3287 (1987).

2. A. Bubenzer, B. Dischler, G. Brandt, and P. Koidl, J. Appl. Phys. **54**(8), 4590 (1983).

3. L. Holland and S.M. Ojha, Thin Solid Films **58**, 107 (1979).

4. C. Weissmantel, in Thin Film Formation from Free atoms and Particles, ed. J. Klabunde, Academic, N.Y., (1985).

5. J.C. Angus, P. Koidl, and S. Domitz, in Plasma Deposited Thin Films, ed. J. Mort and F. Jansen, CRC, Boca Raton, (1986).

6. J.A. Woollam, Hao Chang, and V. Natarajan, Appl. Phys. Commun. **5**, 263 (1985-1986).

7. J.C. Angus and C.C. Hayman, Science **241**, 913 (1988).

8. H. Seki, Surf. Coat. Tech. **37**, 161 (1989).

9. B.V. Spitsyn, L.L. Bouilov, and B.V. Derjaguin, Prog. Crystal Growth and Charact. **17**, 79 (1988).

10. Y. Catherine, and P. Couderc, Thin Solid Films **144**, 265 (1986).

11. E. Staryga, A. Lipinski, S. Mitura, and Z. Has, Thin Solid Films **145**, 17 (1986).

12. F. M. El-Hossary, D. J. Fabian, and C. J. Sofield, Thin Solid Films **157**, 29 (1988).

13. K. Yamamoto, Y. Ichikawa, T. Nakayama, and Y. Tawada, Japanese Journal of Applied Physics **27**(8), 1415 (1988).

14. B. A. Banks, and S. K. Rutledge, J. Vac. Sci. Technol. **21**(3), 807 (1982).

15. D. B. Kerwin, I. L. Spain, R. S. Robinson, B. Daudin, M. Dubus, and J. Fontenille, Thin Solid Films **148**, 311 (1987).

16. K. Tachibana, M. Nishida, H. Harima, and Y. Urano, J. Phys. D **17**, 1727 (1984).

17. K. Kobayashi, N. Mutsukura, and Y. Machi, J. Appl. Phys. **59**(3), 910 (1986).

18. K. Kobayashi, N. Mutsukura, and Y. Machi, Thin Solid Films **158**, 233 (1988).

19. H. S. Butler and G. S. Kino, Phys. Fluids **6**(9), 1346 (1963).

20. B. E. Cherrington, Plasma Chem. Plasma Proc. **2**(2), 113(1982).

21. P. Couderc and Y. Catherine, Thin Solid Films **146**, 93 (1987).

22. M. R. Hilton, G. J. Vandentop, M. Salmeron, and G. A. Somorjai, Thin Solid Films **154**, 377 (1987).

23. J. Robertson, Adv. Phys. **35**, 317 (1986).

24. J. C. Angus, Thin Solid Films **142**, 145 (1986).

25. R. M. Silverstein, C. T. C. Bassler, and T. C. Morrill, Spectrometric Identification of Organic Compounds 4th Ed., John Wiley and Sons (1981).

26. B. Dischler, A. Bubenzer, and P. Koidl, Solid State Comm., **48**, 105 (1983).

27. J. M. Tibbitt, M. Shen, and A. T. Bell, J. Macromol. Sci. Chem., **A10**, 1623 (1976).

28. L. E. Kline, W. D. Partlow, and W. E. Bies, J. Appl. Phys., **65**, 70 (1989).

29. J. R. Conrad and T. Castagna, Bull. Am. Phys. Soc., **31**, 1479 (1986).

30. P. A. Longeway, R. D. Estes, and H. A. Weakliem, J. Phys. Chem., **88**, 73 (1984).

31. C. E. Melton and P. S. Rudolph, J. Chem. Phys., 1771 (1967).

32. F. A. Baiocchi, R. C. Wetzel, and R. S. Freund, Phys. Rev. Lett., **53**, 771 (1984).

33. H. Toyoda, H. Kojima, and H. Sugai, Appl. Phys. Lett., **54**, 1507 (1989).

34. C. Weissmantel, J. Vac. Sci. Technol.**18**(2), 179 (1981).

Table 1. Summary of the mechanical properties of a-C:H films, diamond, and graphite.

8 List of Figures

Fig. 1. Schematic diagram of the plasma deposition and mass analyser system. The substrate can be attached to either electrode. Pressure in the upper chamber is in the mTorr range, while in the lower chamber it is maintained in the 10^{-8} Torr range.

Fig. 2. self-bias voltage vs rf power for our deposition system at a methane pressure of 65 mTorr.

Fig. 3. Plasma potential as it varies between the two electrodes. The powered electrode is at 0 cm and the grounded electrode at 2 cm. Potentials are based on Langmuir probe measurement and ion energy distributions. Boundaries between the glow region and the ion sheaths or dark spaces are based on visual inspection.

Fig. 4. Deposition rate vs rf power for the powered and grounded electrodes. Data points were taken for the powered and grounded electrodes in both upper and lower positions in the deposition apparatus to show the symmetry with respect to gas flow.

Fig. 5. Secondary electron microscope images of scratch tracks made with a Rockwell C diamond tip at a load of 831g, for films formed on the powered and grounded electrodes. Little damage is apparent on the hard film formed on the powered electrode, while the soft film formed on the grounded electrode has suffered noticeable damage.

Fig. 6. Peak to peak auger intensities for carbon and silicon as a function of argon ion sputter time for areas in the scratch track and away from the scratch track of the areas shown in Fig. 5. A large amount of intermixing is evident in the scratch track of the soft film formed on the powered electrode.

Fig. 7. FTIR spectra of a-C:H films formed on the grounded (a, b) and powered (c, d) electrodes in the regions of interest for CH bending (a, c) and CH stretching (b, d). Film thicknesses for the grounded electrode and powered electrode films are 1.27 μm and 2.15 μm, respectively. Spectra for the film formed on the grounded electrode shows absorptions due to CH_3 not apparent in the powered electrode film spectra.

Fig. 8. Mass spectra of neutrals incident on the grounded electrode (GE), and the powered electrode (PE).

Fig. 9. Experimental and calculated intensities of the mass spectrometric signals in the cracking of various C_2H_x species. Intensities are calculated based on the optimum concentration ratios (calculated as C_2H_6 : C_2H_4 : C_2H_2 = 0.45 : 0.27 : 0.28) and the cracking pattern spectra of the pure gases taken with the same apparatus.

Fig. 10. Partial pressures of neutral species above the substrates at the grounded electrode (GE), and the powered electrode (PE).

Fig. 11. Relative intensities of 12 - 15 mass signals due to neutral radical species, for the grounded electrode (GE), and the powered electrode (PE). The CH_3 radical is the predominant radical species in the plasma.

Fig. 12. Effect of direct path shielding on the detected neutral radical intensities. Intensities with a shield and with no such shield are shown. The lack of a measurable change in the 15 amu signal intensity indicates a small sticking coefficient for the methyl radicals with the chamber walls.

Fig. 13. Mass spectra of ions incident on the grounded electrode (GE) and the powered electrode (PE). The intensity for the grounded electrode spectrum is magnified by a factor of ten.

Fig. 14. Ion signal intensity vs ion energy for the total ions, H_2^+, and CH_3^+ ions incident on the grounded electrode (open shapes) and the powered electrode (solid shapes). The energies with which the ions strike the powered electrode are 350 eV greater than those measured at the mass spectrometer and listed here.

Fig. 15 The dependence of deposition rate (a), and of hardness and compressive stress (b) on the time averaged potential drop between the plasma bulk and the substrate. Hardness depends monotonically on the average potential drop between the plasma and the electrode, ie the power delivered to the film surface by ions, as controlled by pulsed biasing. Deposition rate is independent of the average potential drop. The pulse frequencies are 25, 12.5, and 6.25 kHz for the -800 V pulses (●), 25 and 12.5 kHz for -1100 V (◘), 25 kHz for -500 V (O) and -200 V (▵), and 100kHz for -20 V (▲) and -80 V (■). The symbols are listed in the brackets behind each peak voltage, with 0 V being (△).

Fig. 16. Effect of nitric oxide addition on the deposition rate at the powered electrode (PE) and the grounded electrode (GE). Radical scavenging by NO decreases the deposition rate dramatically.

Fig. 17. Mass spectra of ions incident on the powered electrode for 0% NO feed gas concentration and for 20% NO. The presence of the radical scavenger has a relatively small effect on ion flux.

Table 1. Summary of the mechanical properties of a-C:H films, diamond, and graphite.

	a-C:H (50W rf Power)		Diamond	Graphite
	PE	GE		
Density (g/cm3)	1.6 - 1.8	1.2 - 1.4	3.52	2.27
Hardness (GPa)	33 - 35	~2	~100	--
Stress (GPa)	1.5 - 3.0	~0	0	0

* 1 GPa = 102 Kg/mm^2

XBL 896-2531

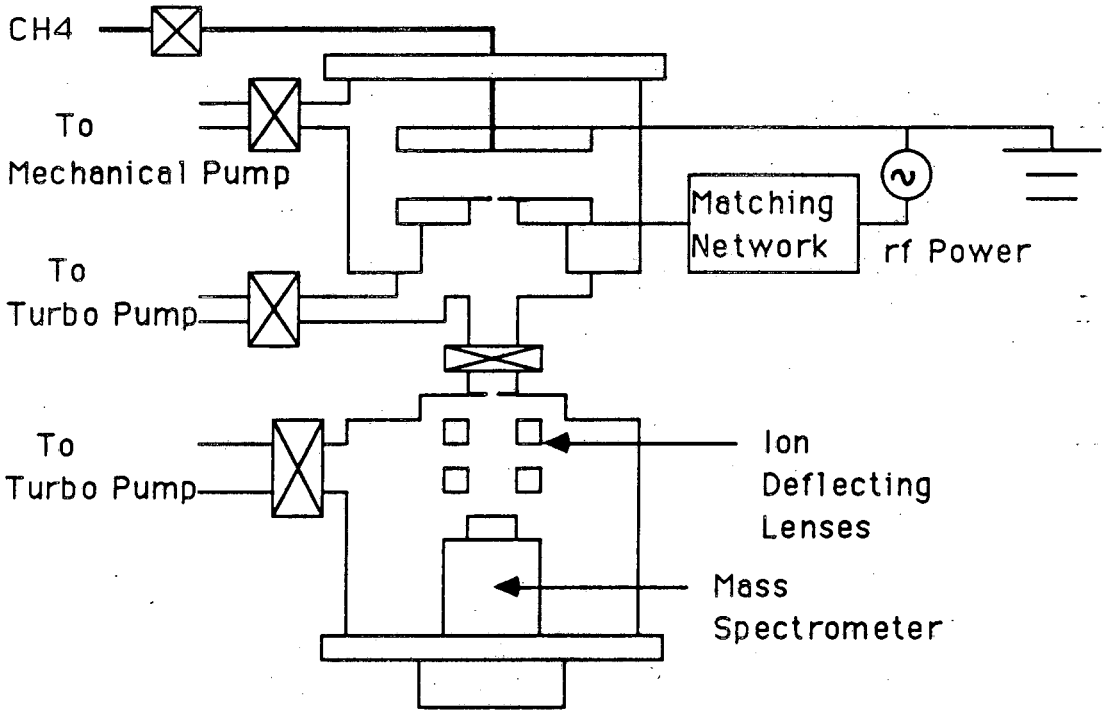
CH4
To
Mechanical Pump
To
Turbo Pump
To
Turbo Pump
Matching
Network
rf Power
Ion
Deflecting
Lenses
Mass
Spectrometer

Fig. 1

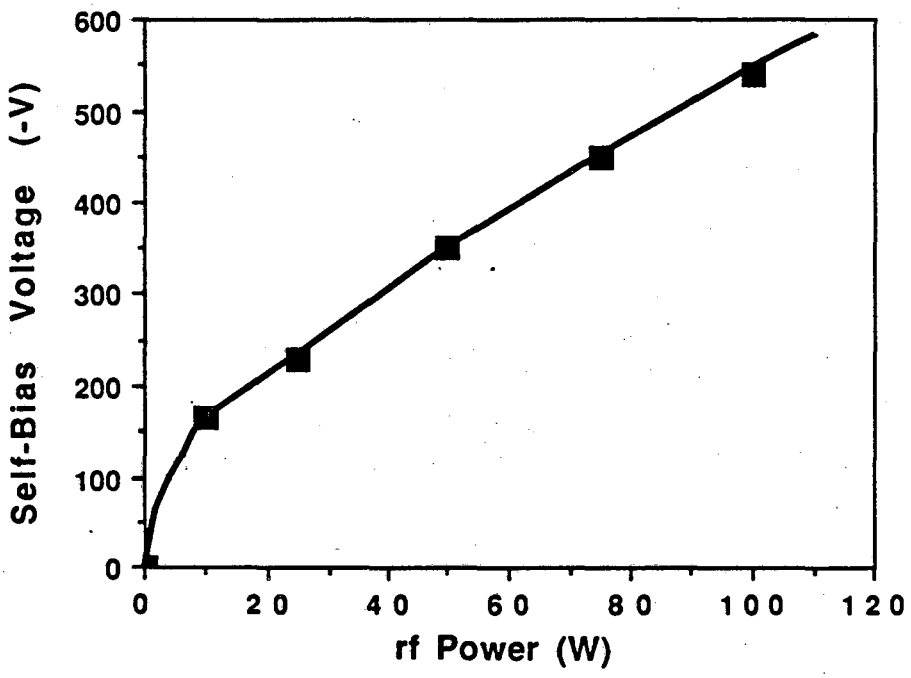
Self-Bias Voltage (-V)
600
500
400
300
200
100
0
0
20
40
60
80
100
120
rf Power (W)

Fig. 2

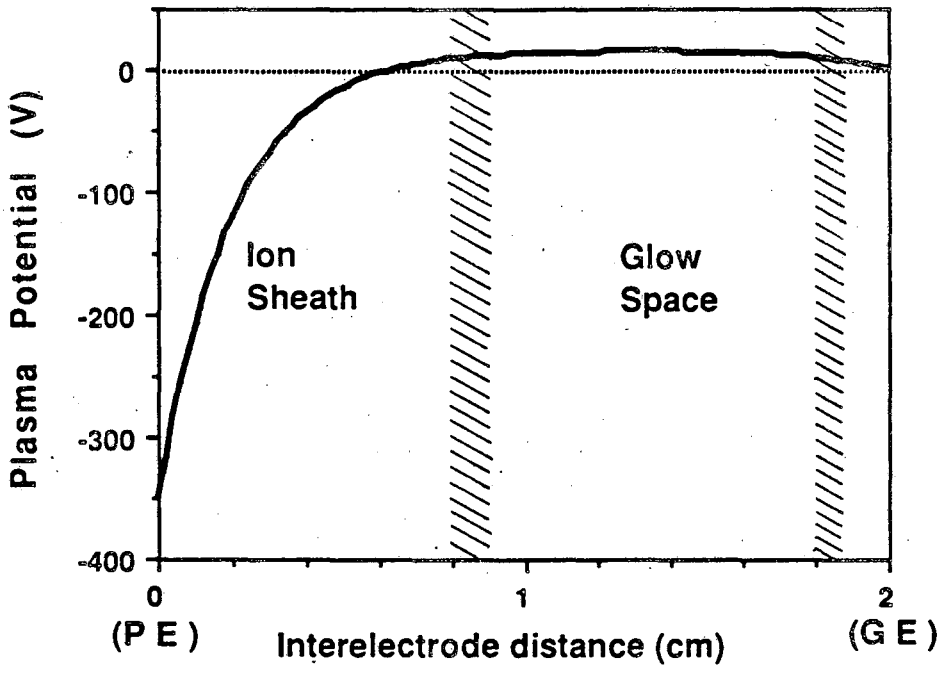
Plasma Potential (V)
0
-100
-200
-300
-400
Ion
Sheath
Glow
Space
0
(P E)
1
2
(G E)
Interelectrode distance (cm)

Fig. 3

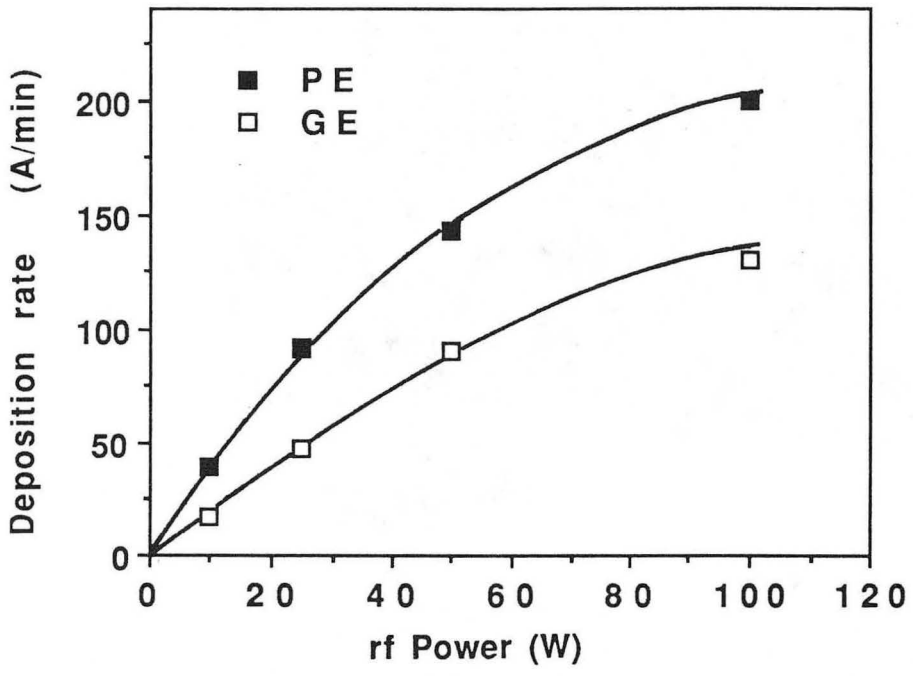
PE
GE
Deposition rate (A/min)
200
150
100
50
0
0
20
40
60
80
100
120
rf Power (W)

Fig. 4

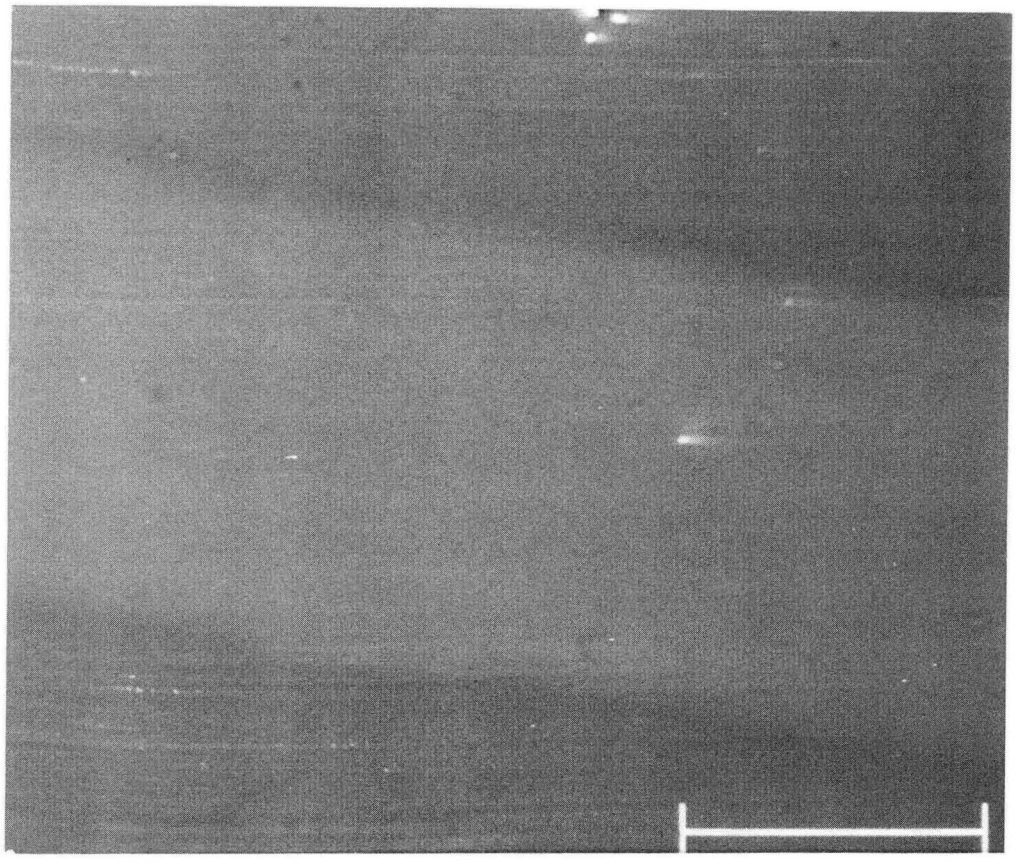

PE

50μm

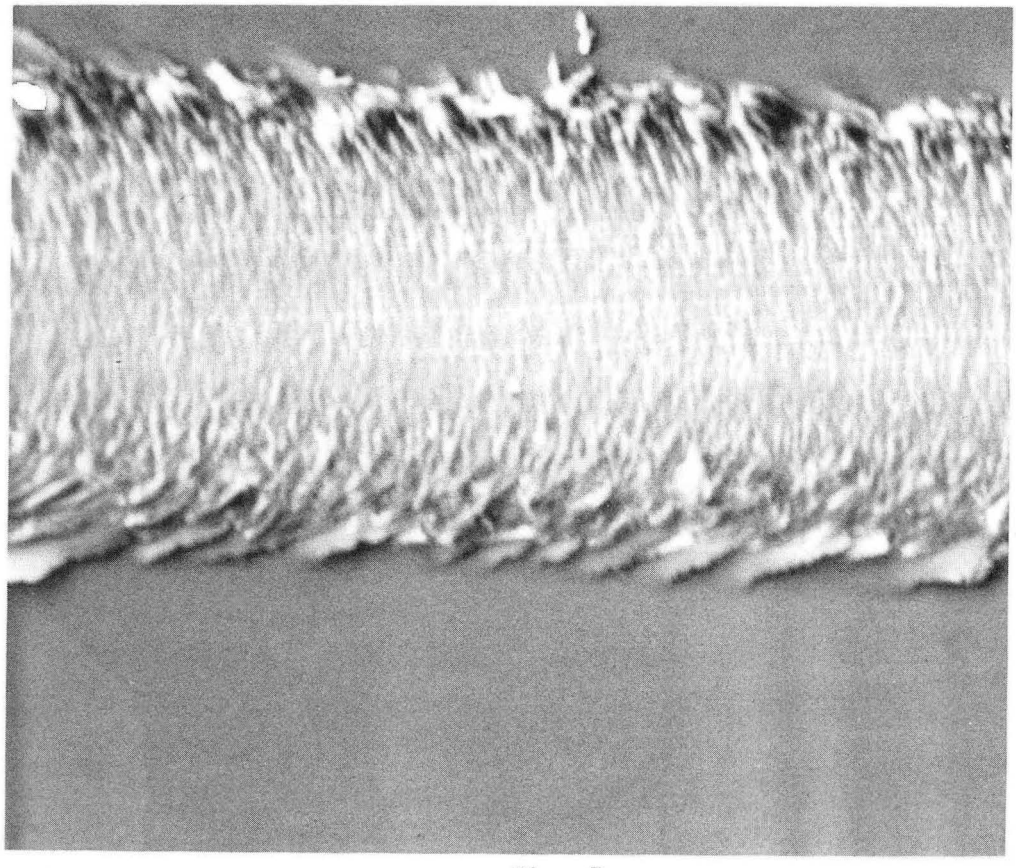

GE

Fig. 5

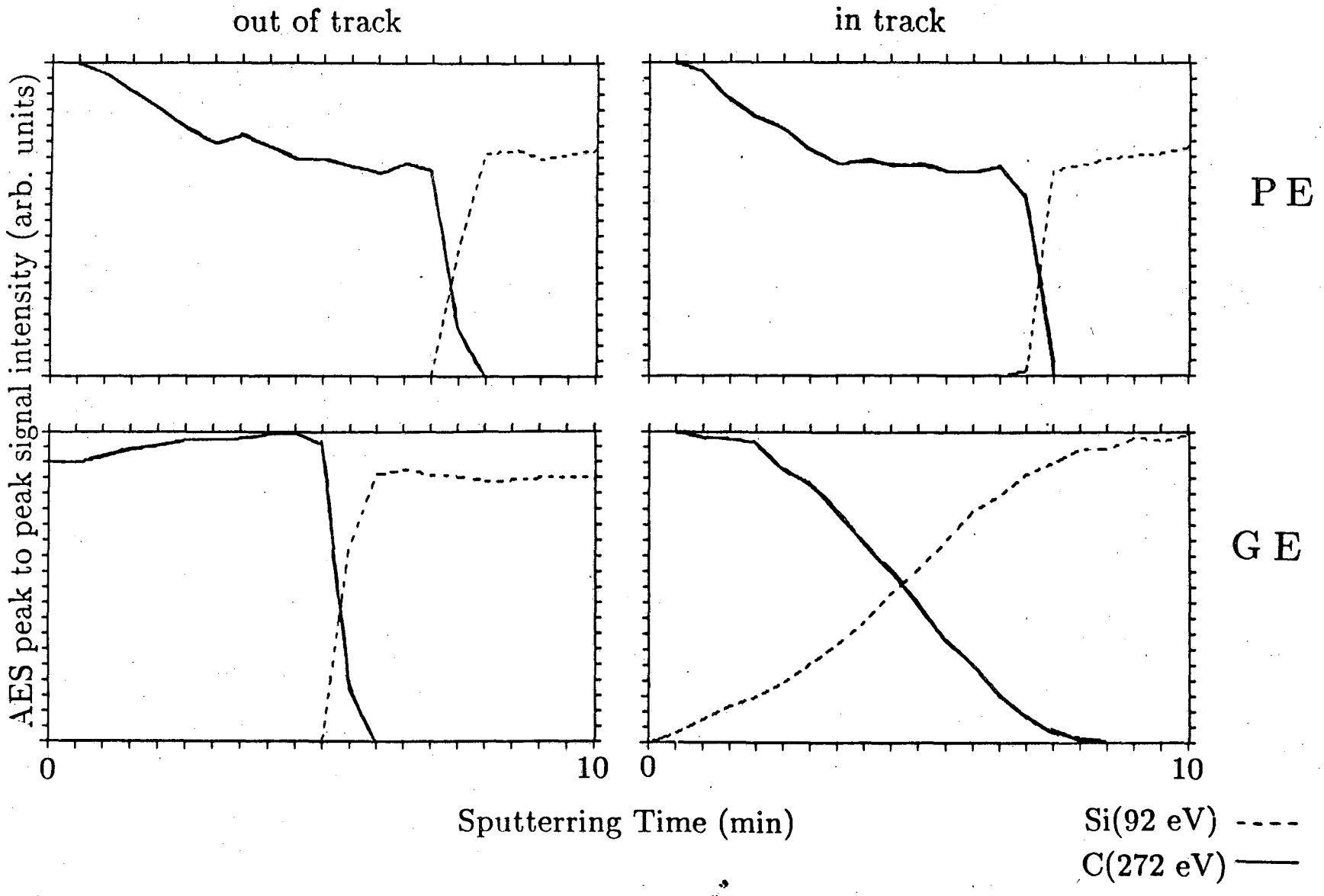
out of track
in track
AES peak to peak signal intensity (arb. units)
P E
G E
0
10
0
10
Sputterring Time (min)
Si(92 eV) ----
C(272 eV) ——

Fig. 6

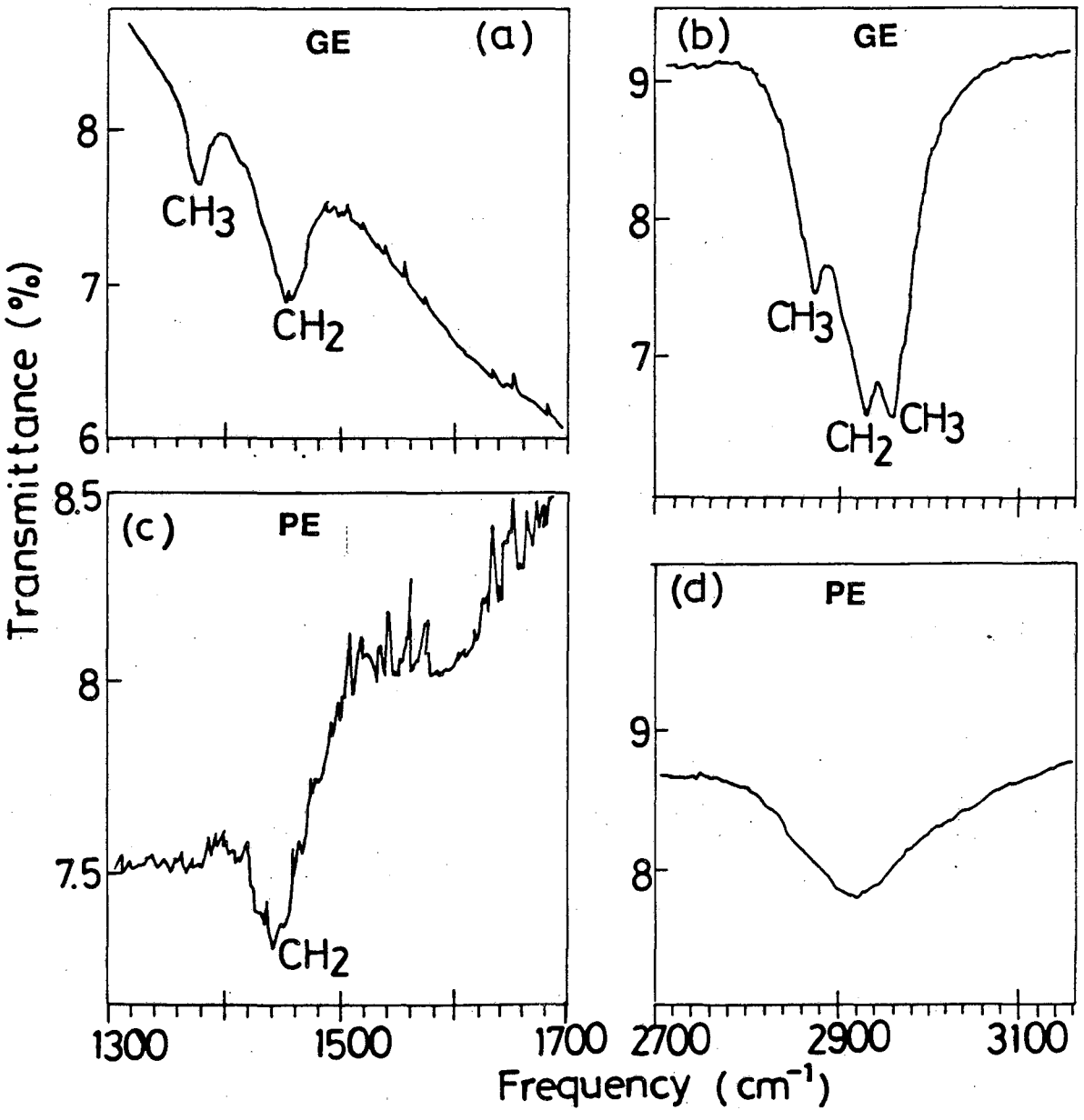

XBL 896-2532

Fig. 7

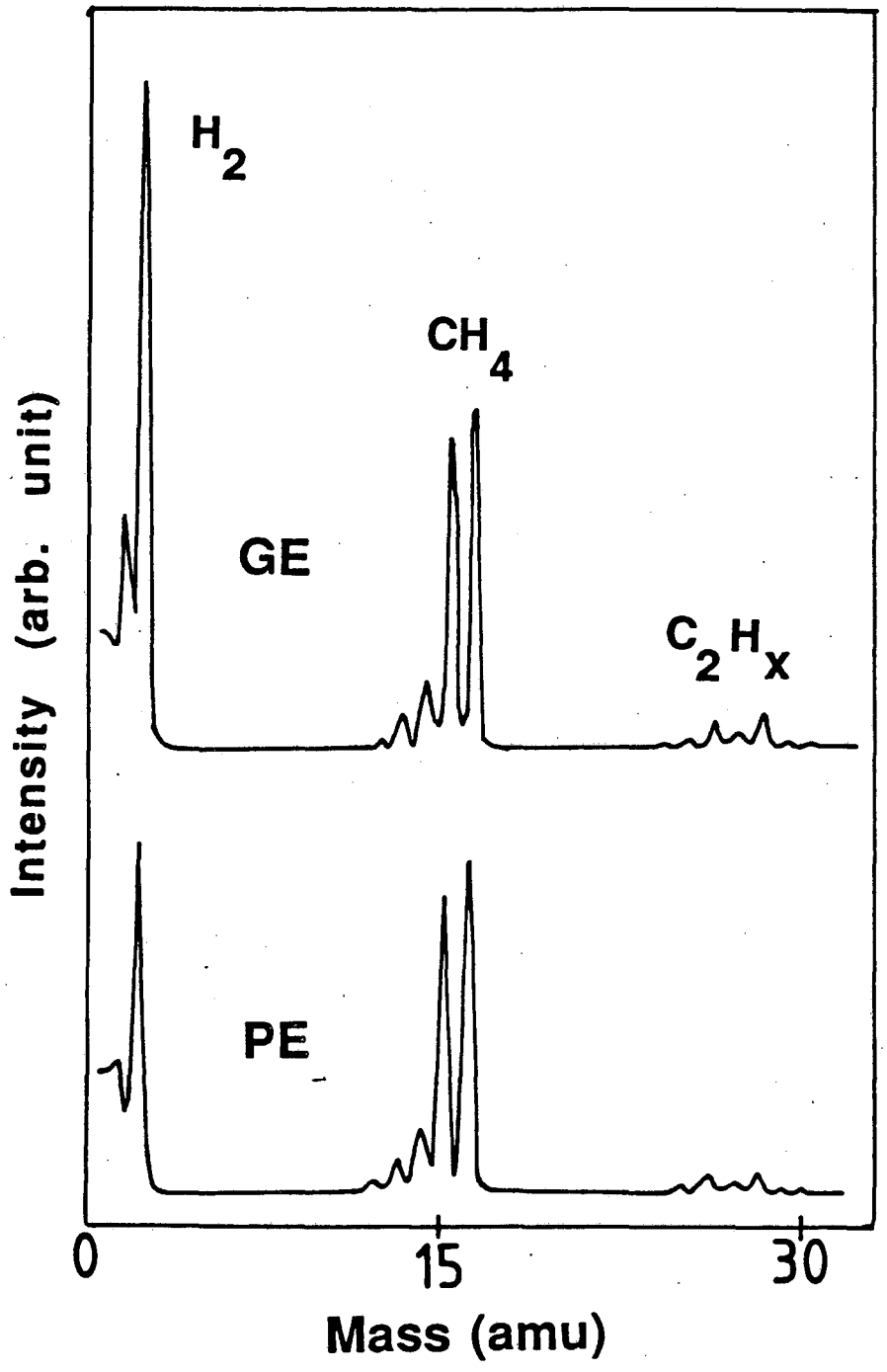

XBL 896-2533

Fig. 8

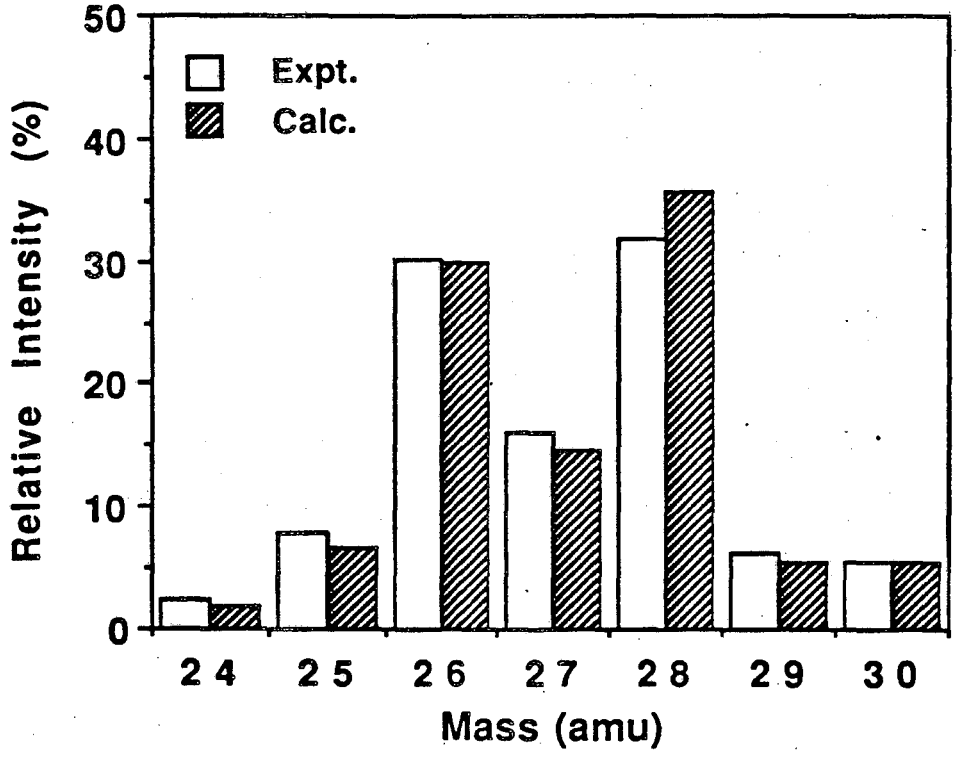
Expt.
Calc.
Relative Intensity (%)
50
40
30
20
10
0
24
25
26
27
28
29
30
Mass (amu)

Fig. 9

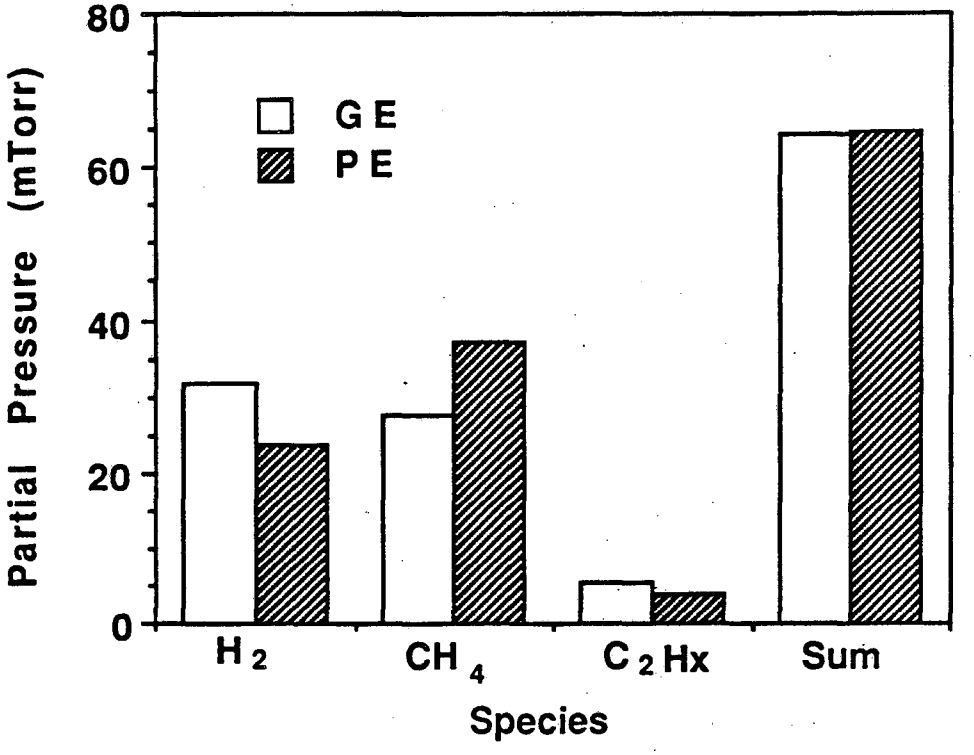
80
60
40
20
0
Partial Pressure (mTorr)
G E
P E
H 2
CH 4
C 2 Hx
Sum
Species

Fig. 10

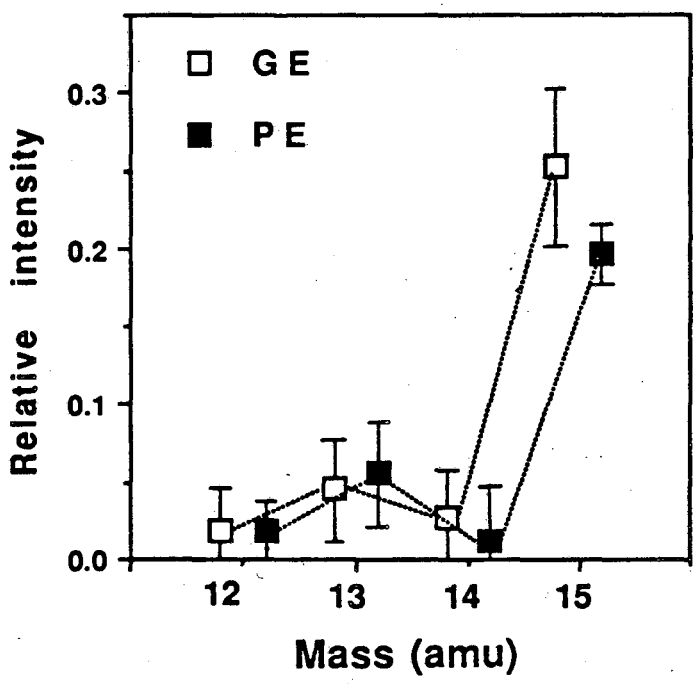

Fig. 11

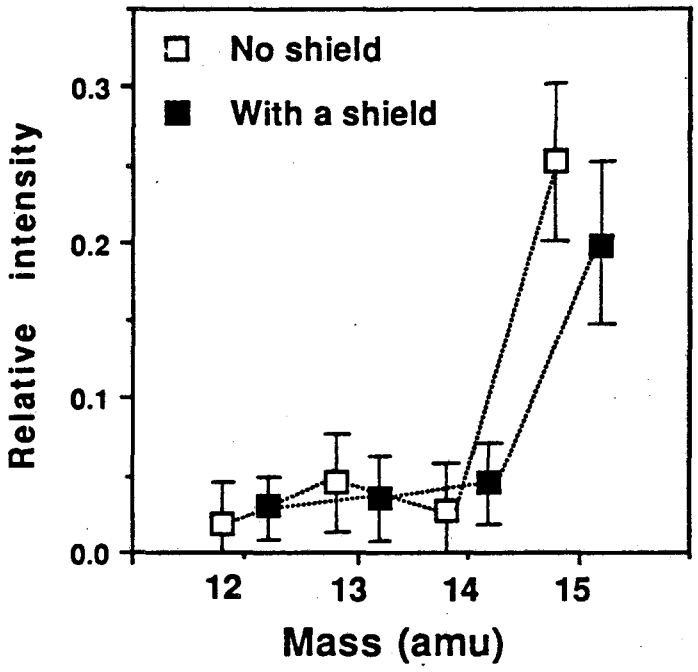
No shield
With a shield
Relative intensity
0.3
0.2
0.1
0.0
12
13
14
15
Mass (amu)

Fig. 12

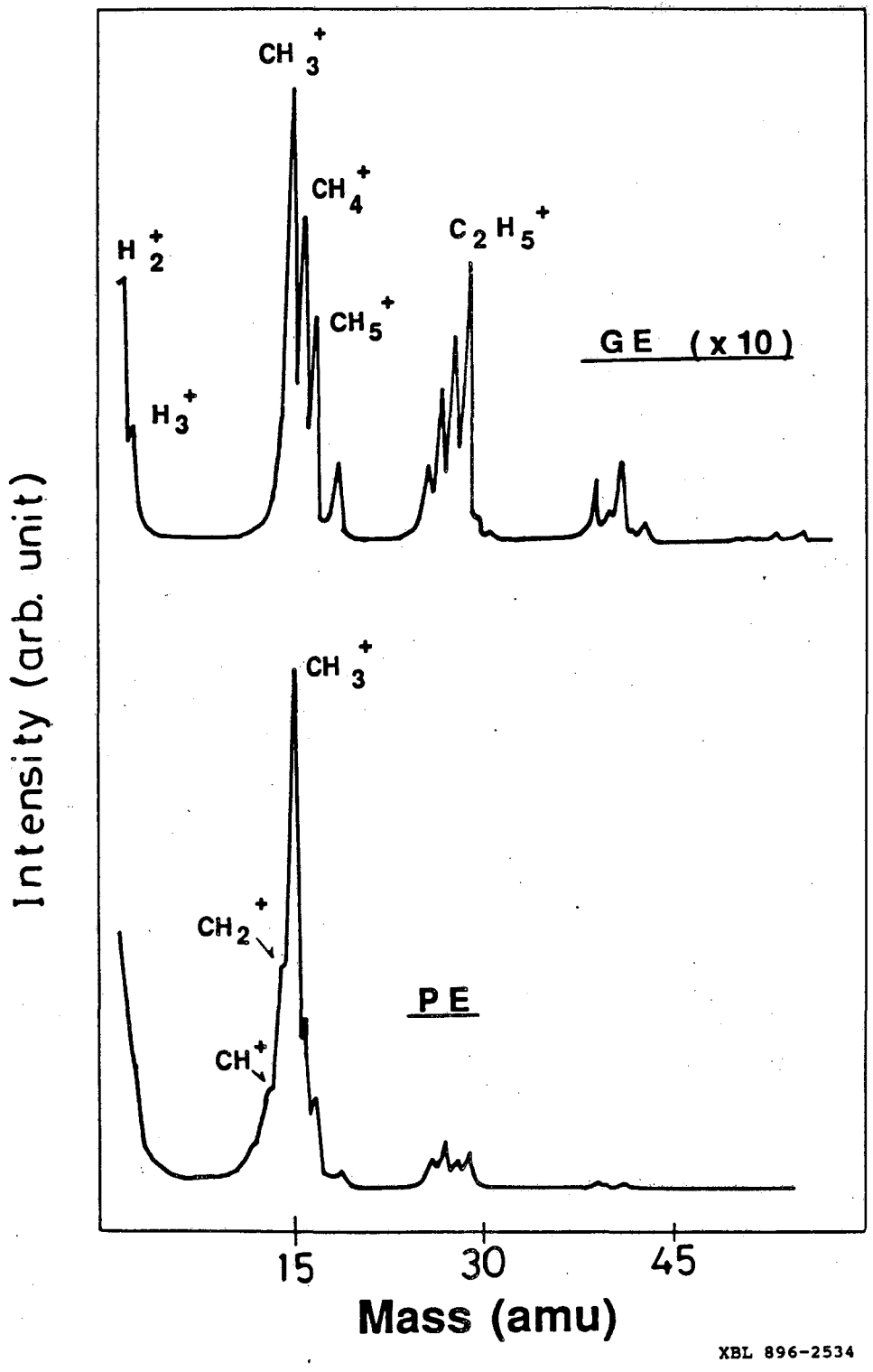
CH 3+
CH 4+
C2 H5+
H 2+
CH5+
GE (x10)
H3+
Intensity (arb. unit)
CH 3+
CH2+
PE
CH+
15
30
45
Mass (amu)
XBL 896-2534

Fig. 13

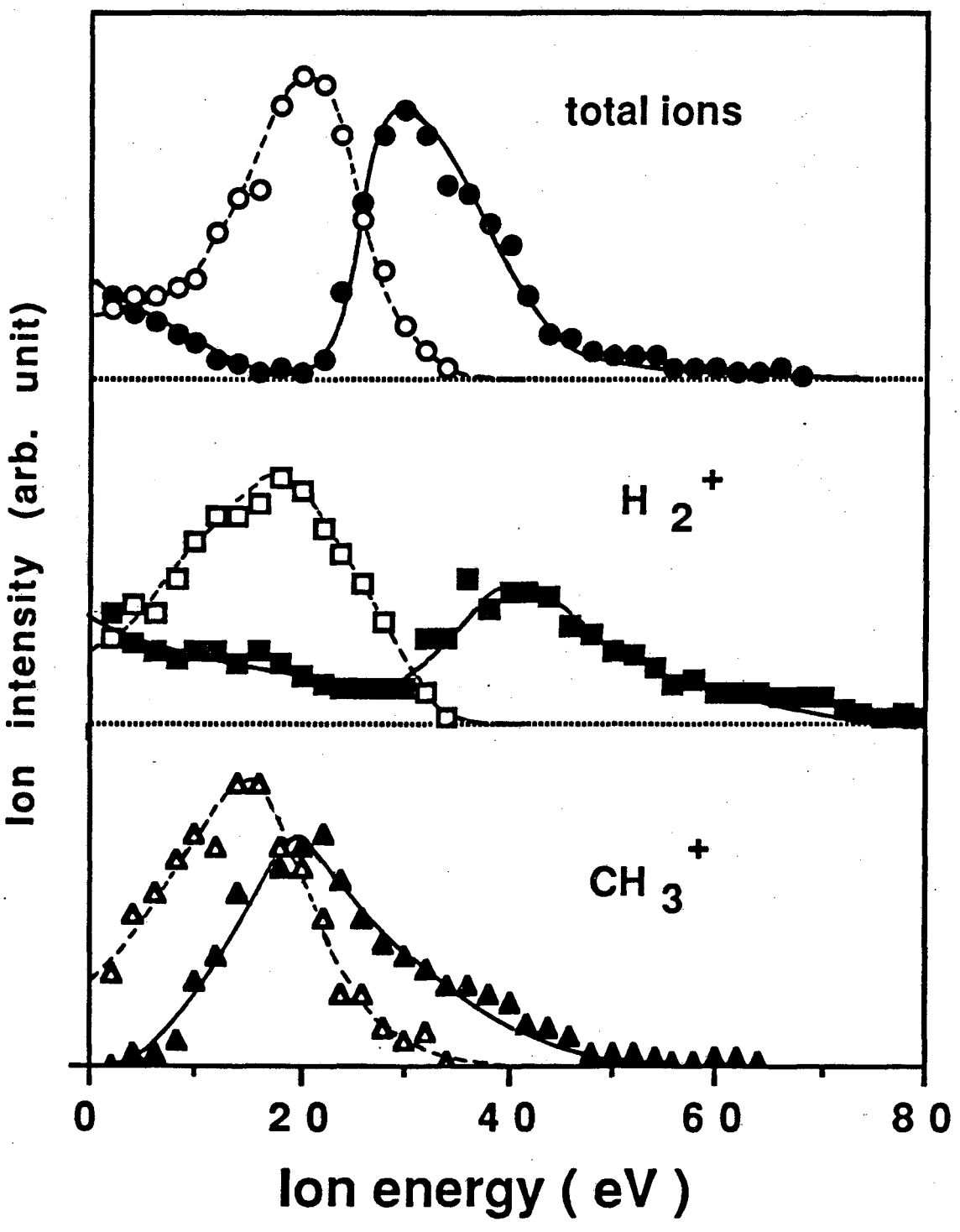

XBL 896-2535

Fig. 14

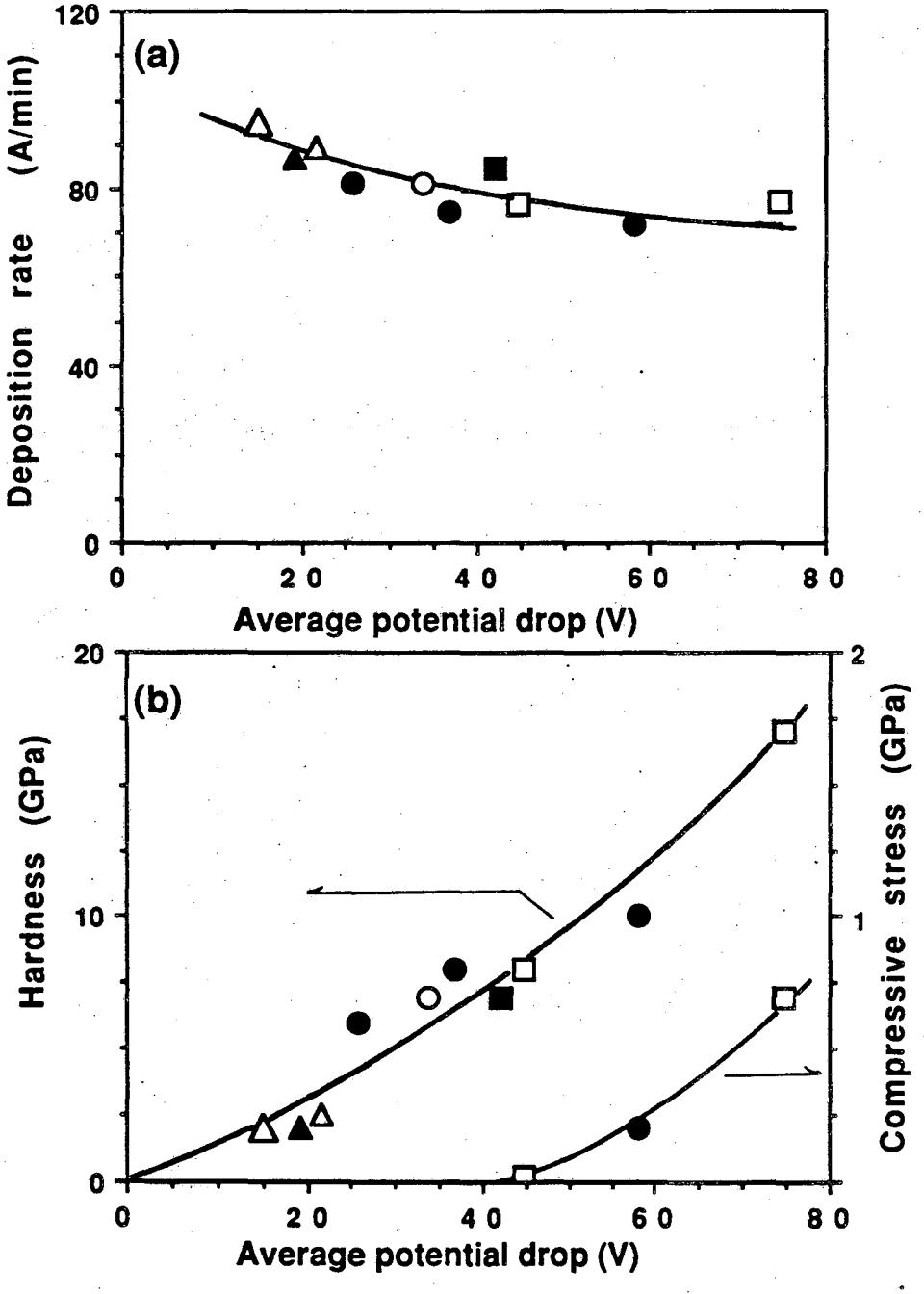
(a)
Deposition rate (A/min)
120
80
40
0
0
20
40
60
80
Average potential drop (V)
(b)
Hardness (GPa)
20
10
0
Compressive stress (GPa)
2
1
0
20
40
60
80
Average potential drop (V)

Fig. 15

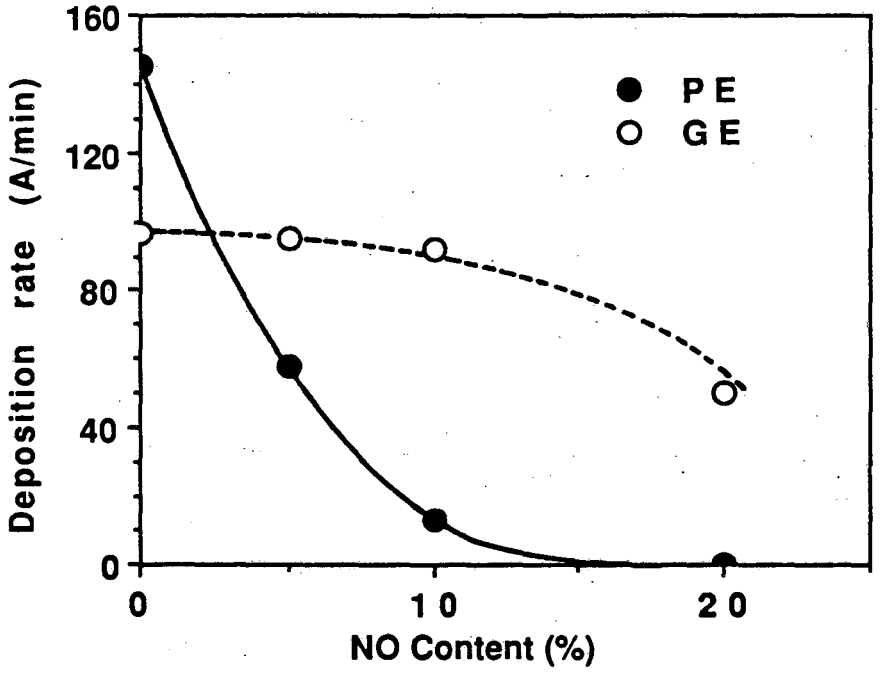

Fig. 16

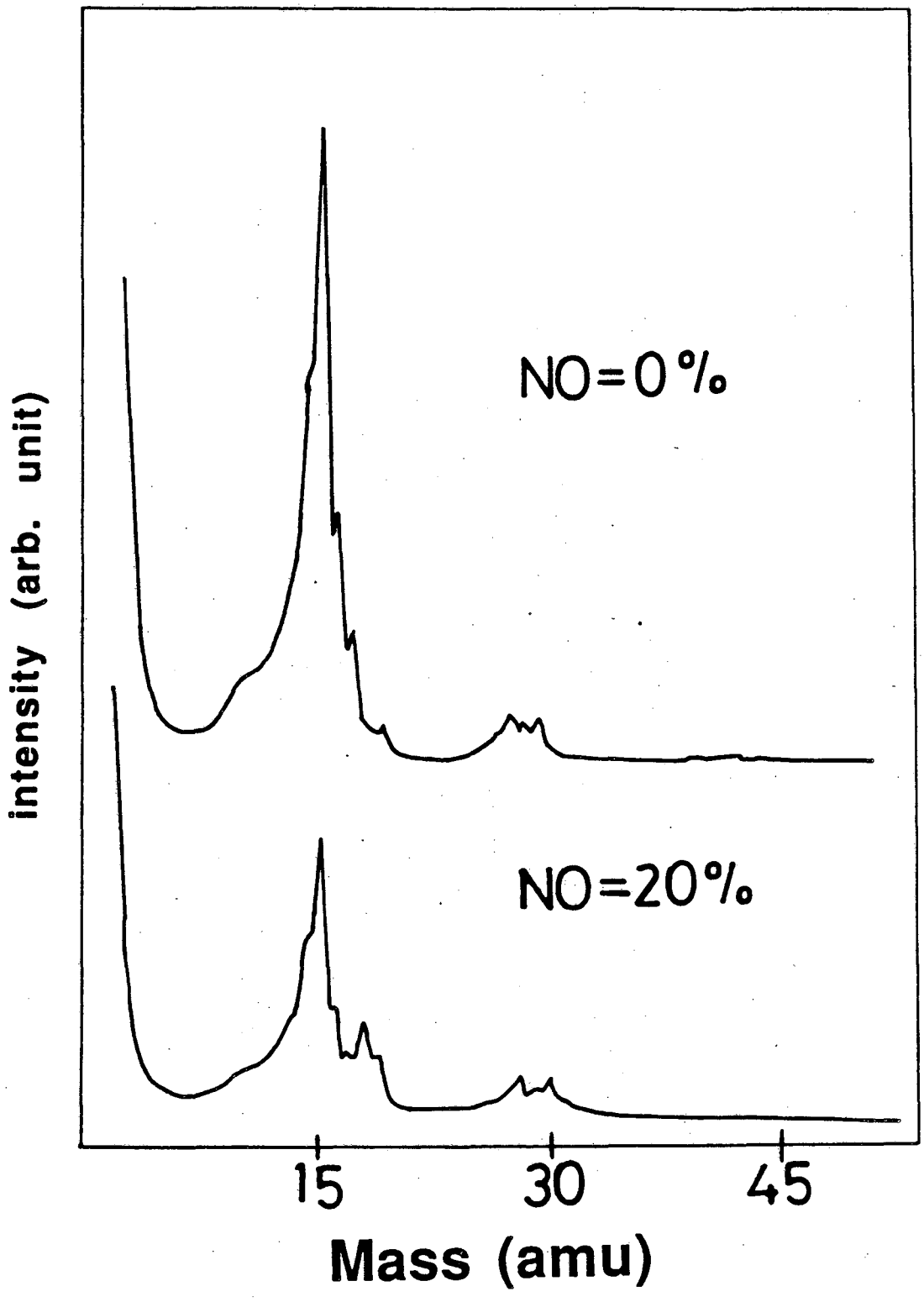

Fig. 17

LAWRENCE BERKELEY LABORATORY
CENTER FOR ADVANCED MATERIALS
1 CYCLOTRON ROAD
BERKELEY, CALIFORNIA 94720